Advances in Experimental Mechanics Related to Novel Materials Tested under Monotonic and Cyclic Loading Conditions

Zbigniew L. Kowalewski[1], Mateusz Kopec[1] & Aneta Ustrzycka[1]

Abstract: This paper presents several attempts to use novel optical techniques for damage evaluation of materials subjected to either monotonic or cyclic loading and its monitoring on specimens made of the nickel super-alloy and power engineering steel. Effectiveness in damage analysis of Digital Image Correlation (DIC) and Electronic Speckle Pattern Interferometry (ESPI) is compared.

Keywords: Fatigue; Damage; Optical full-field methods

1. Introduction

The most conventional method for material testing includes extensometer recordings during static, monotonic and cyclic loading. Such methodology enables continuous recording of strain changes in a particular direction defined at the beginning of mechanical test. It can only monitor a displacement on the limited strain gauge, and more importantly, give only an average value of it. This is a serious limitation of the technique, particularly in the case of fatigue investigations. Although fatigue phenomenon has been investigated by many research centres for more than 200 years, there are still a lot of difficulties in prediction of crack initiation under cyclic loading. It is well known that the process of the fatigue damage development and structural degradation is of local nature, and as a consequence, an application of the above mentioned conventional extensometers for strain measurements cannot reflect strain distribution along the gauge length of specimen tested. Indication of a point of crack initiation within the gauge length is practically impossible using the conventional extensometers. Such a problem may be effectively solved by application of either ESPI (Electronic Speckle Pattern Interferometry) [1] or DIC (Digital Image Correlation) full-field optical methods [2, 3].

   ESPI is the holographic interferometry type technique based on the laser beam analysis distracted from the optically rough surface. The specimen surface is captured as an image by the CCD (charge-coupled device) sensor and transferred to a working station. As the first beam illuminates the specimen surface, the reflected beam interferes with the reference beam, and thus, the subtraction process of the speckle interferograms (before and after loading up to the defined levels) is performed and correlation fringes are obtained. The fringes enable to generate a phase map with distribution of displacement components in each direction, separately [4]. Subsequent

mathematical operations under the fixed boundary conditions (measurement area dimensions) and the material parameters (Young's modulus and Poisson's ratio) led to the final full-field stress and strain phase maps. ESPI, although different in terms of operation principles, it is quite similar to DIC optical technique for which also the displacement maps during loading can be obtained. It should be mentioned however, that it has significantly higher than DIC resolution. More importantly, it is mainly laboratory scale dedicated due to a high vibration sensitivity, that disturbs seriously the results captured.

DIC is a stereoscopic technique in which two CCD cameras, light sources and computational software are used. A mathematical theory of DIC was presented by Chu et al. [5]. In this method, a specimen needs to be covered with a special pattern (black dots on a bright background) [5, 6]. Such pattern defines the x and z coordinates which are further used to run the test under the strain control. Origins of rectangular or square shaped pattern are directly applied to calculate the displacement/strain. The results obtained are presented in the form of full-field, strain distribution maps [6]. DIC method is mainly used for static measurements in which tensile and compressive behaviour [7], fracture toughness [8] and the geometrical imperfection effects on mechanical response [6] can be investigated in detail.

Both ESPI and DIC have many applications. DIC was used to study different kinds of materials, such as soft and hard biological tissues [9-12], dental materials [13] or materials for high temperature applications [14]. It was also applied for structural dynamics assessment [15], residual stress and its error estimation [16], in situ monitoring of additive manufacturing [17], and many others. On the other hand, ESPI has been recently employed for assessing the integrity of structural materials, evaluating residual stress fields in pipes, measuring surface displacements during inflation testing of ocular tissues or to assessing strain in bone-implant interfaces [18].

This paper presents several attempts to use such techniques for damage evaluation of materials subjected to different types of loading.

2. Materials and Methods

Two types of plane specimens were tested. The first one, just the standard, and the second with a hole located in the central part of the gauge length. Engineering drawings of specimens designed for fatigue tests are shown in Fig. 1.
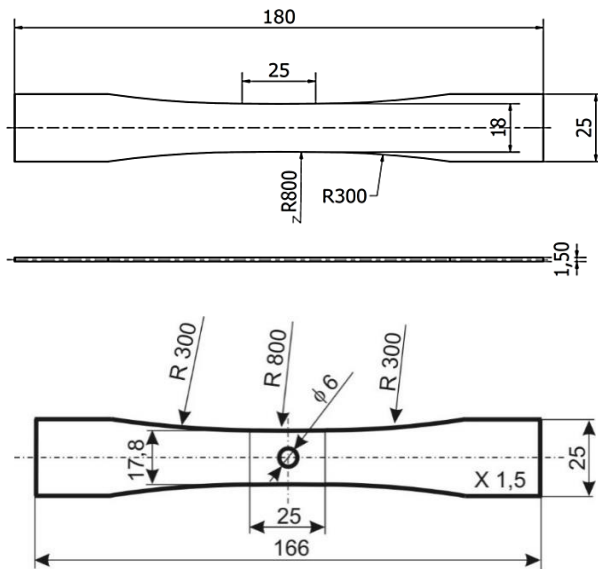Two kinds of materials were tested. The specimens of the first material were manufactured using X10CrMoVNb9-1 (P91) polycrystalline steel. This is a low carbon, creep-resistant steel, typically used for tubes, plates and structural components in the power plant industry. The content of alloying elements in P91 includes C $(0,2 \div 0,5\%)$; Mn $(0,3 \div 0,6)$; Cr $(8 \div 9,5)$; Mo $(0,85 \div 1,1)$; V $(0,18 \div 0,25)$; Ni $(< 0,4)$; Cu $(< 0,3)$; Si $(0,08 \div 0,12)$; S $(< 0,01)$. The specimens of the second material in question were produced applying nickel super-alloy of the following chemical composition: C – 0.09%, Cr – 8.8%, Mn – 0.1%, Si– 0.25%, W– 9.7%, Co – 9.5%, Al – 5.7%, Ta+Ti+HF– 5.5%.

The fatigue tests for both tested materials were force controlled with zero mean level and a constant stress amplitude with a frequency of 10 Hz or 20 Hz using the
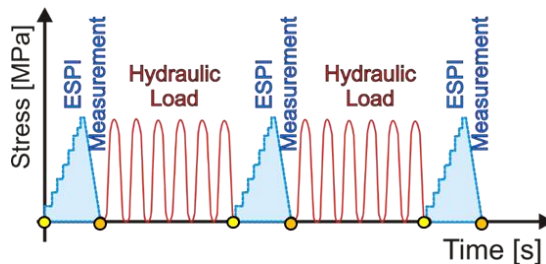
MTS-810 hydraulic testing machine. The tests for P91 steel were carried out in the range of stress amplitude from ±380 MPa to ±640 MPa. In the case of nickel super-alloy in each test the maximum cyclic stress range and stress amplitude were equal to 600 MPa and 300 MPa, respectively. Both these parameters were lower than the yield point of the material in question.

The fatigue development was monitored by Dantec Dynamics Q100 ESPI system and DIC Aramis 12M equipped with lenses of total focal length of 75 mm and calibration settings appropriate to the measuring area equal to 170x156 mm.

In order to eliminate vibrations of the testing machine during ESPI optical measurements, the loading process of the specimen was executed manually using a special device designed originally by the IPPT PAN workers. The loading program is presented in Fig. 2.

Fig. 1. The geometry of the specimens: (a) typical plane; (b) with central hole in the middle of gauge length (units are in mm).

Fig. 2. Loading program for cyclic loading tests supported by ESPI system.

3. Results

3.1. The results for the P91 steel

The purpose of tests on P91 steel was to provide experimental data on the evolution of micro-strain regime during high cycle fatigue crack initiation. The whole fatigue process was divided on the blocks of cycles and carried out using the hydraulic servo-controlled testing machine. The process of cyclic loading was interrupted several times after selected numbers of cycles in order to perform displacement measurements by means of the ESPI camera. Strain distribution maps at the maximum load applied on the plane specimen surface using ESPI are presented for increasing number of the loading cycles in Figs. 3, 4, 5 and 6. Three types of specimens were tested: specimen with relatively rough surface, electropolished specimen and specimen with the hole. The different stages of the fatigue process, from the beginning up to the moment of crack initiation and subsequent propagation are presented. During the process of cyclic loading the material deforms heterogeneously and numerous strain concentration spots are visible in the case of rough specimen, Fig. 3. The lateral profiles of the maximal cross-sectional strain distribution for increasing cycles number for rough specimen on the surface are presented in Fig. 4. It is expected that the microstructure of the material plays an important role in the strain localization. In order to reduce roughness and remove some modification of the material properties resulting from electro-machining (local heating-cooling), the surface of specimen was electro-polished in the vicinity of cracks generated in the fatigue process. The strain distribution maps are presented in Fig. 5a. The lateral profiles of the maximal cross-sectional strain distribution for increasing cycles number for electropolished specimen are presented in Fig. 5b. As it is seen from the profiles, Figs. 4 and 5b, the places of damage initiation are easy for identification. They are well represented by the significant increase in strain.
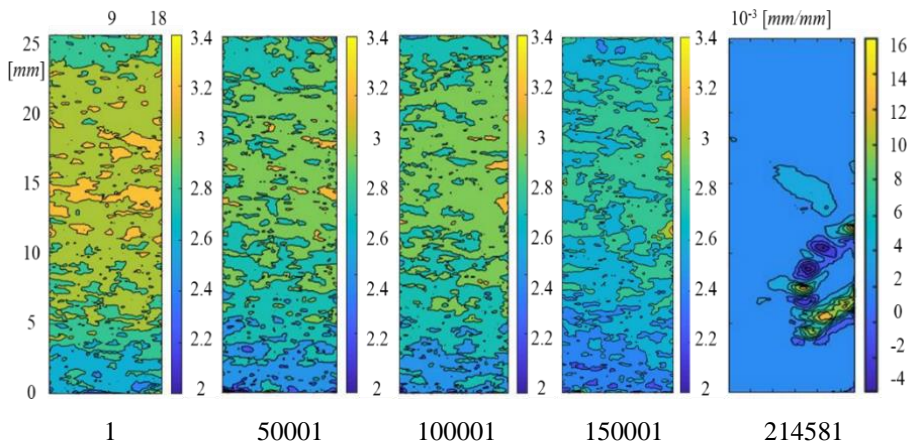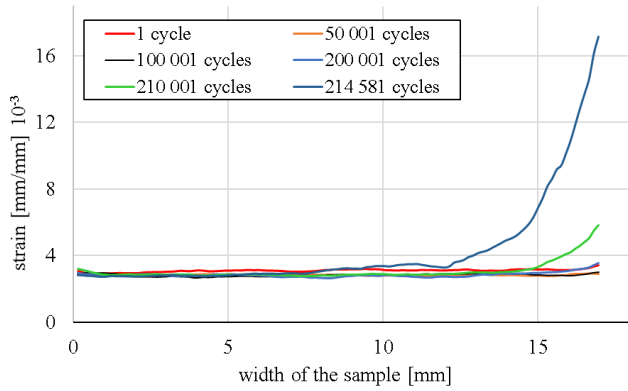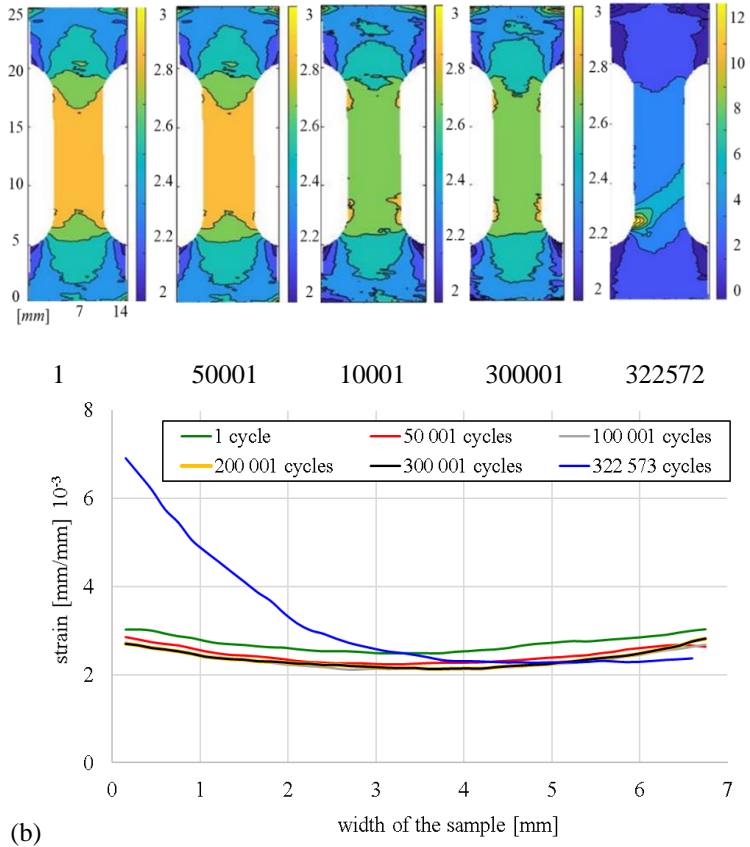

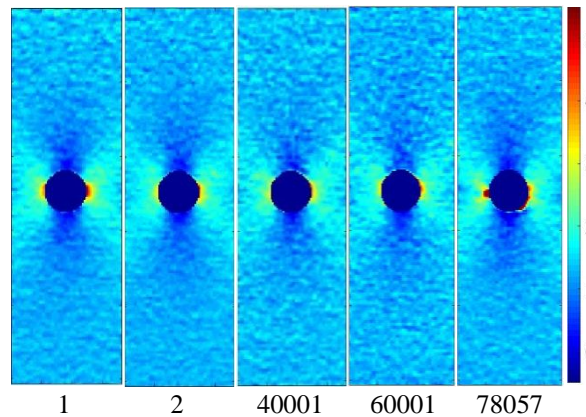**Fig. 3.** Strain distribution maps - rough specimen on the surface

Fig. 4. Lateral profiles of the maximal cross-sectional strain evolution

(a)

(b)

Fig. 5. Strain distribution maps - electropolished specimen (a), and the lateral profiles of the maximal cross-sectional strain evolution (b)

In the case of specimen with the hole, in the first cycle the strain accumulation spot is visible near the hole, (Fig. 6, 1 cycle). In the next cycles the material is strengthened (Fig. 6, 2 cycles), but the local zones of strain accumulation in the vicinity of the hole can be still observed, however, they have a slightly lower level in comparison to the first cycle. The crack localisation on the left side of the hole is presented in Fig. 6 after 78057 cycles.
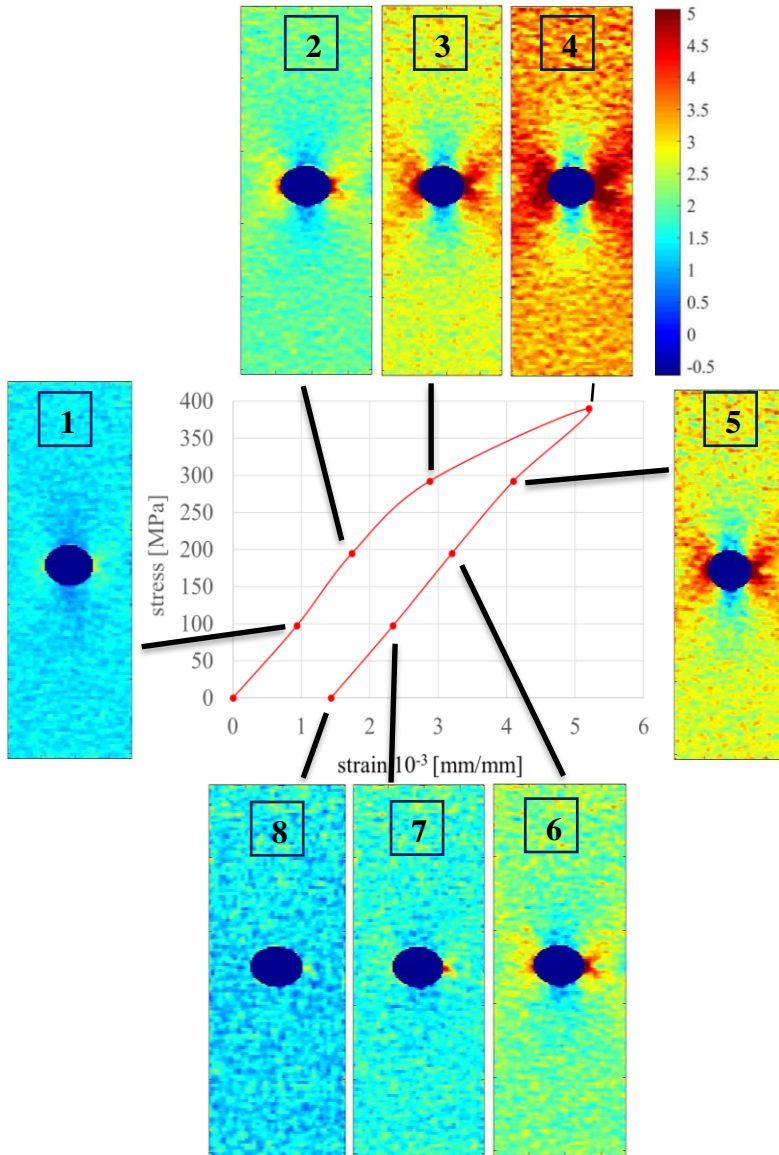

Fig. 6. Strain distribution maps - specimen with the hole

Introduction of a geometric discontinuity in the form of the hole in the central part of specimen introduces advantageous condition (stress and strain concentrations) for crack initiation. On the basis of strain fields specified for different forces a local hysteresis curve can be generated for selected points of the specimen, (Fig. 7 (1-8)). The local stress cannot be measured directly in the experiment, however, the hysteresis curve shows the nominal stress versus local strain.

The latter corresponds to the maximum stress/strain concentration point. The aim of the experiment was to follow the distribution of local strain fluctuations during a loading/unloading cycle. The strain distribution maps corresponding to the selected points of the curve are also presented in Fig. 7. Near the hole, the local zone of strain concentration was created. As shown in Fig. 7 (3, 4, 5), during specimen loading, the strain concentration occurs in shape of "V". Two plasticity bands inclined at certain angle are created. The initial state of fatigue crack nucleation mechanism begins by a formation of shear bands. This is a result of deformation mechanism that localizes large shear strains. As a consequence of the inhomogeneous plastic deformation at the root of the hole, the residual strain is left on the surface, Fig. 7 (8).

The ESPI results in the form of local strain values are in good agreement with the numerical results that can be found in [1].
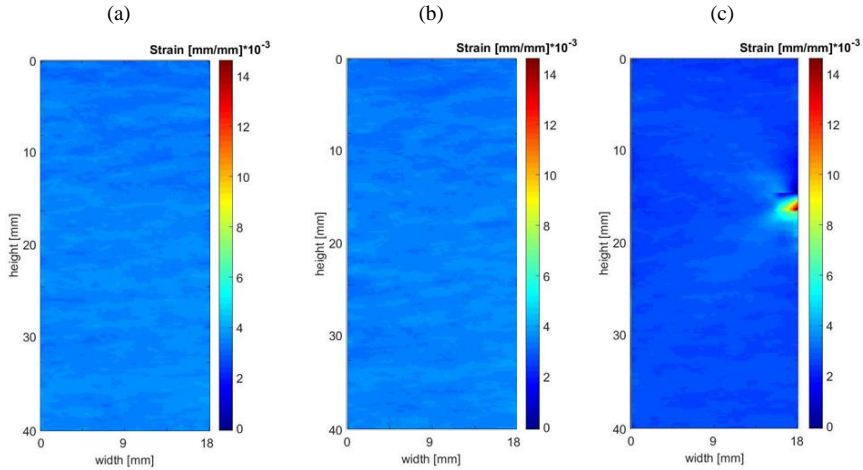
Fig. 7. Hysteresis curve showing the single loading cycle paused at selected stress levels during the strain distribution maps capturing

In order to check the effectiveness of the ESPI method, additional tests were performed under the same conditions on the plane specimens without holes using also Digital Image Correlation (DIC). Each specimen fractured within 1000 cycles from the crack initiation. It should be highlighted, that the ESPI measurements enabled to
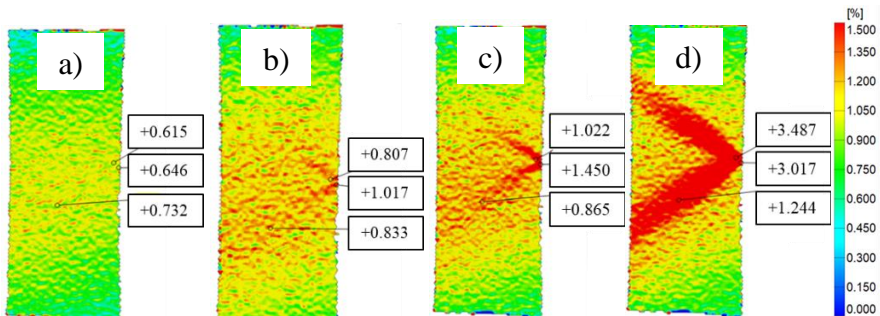
observe damage almost close to the specimen fracture only. In order to better recognition of this problem, tests were also performed for the stress amplitudes equal to 550 MPa, 600 MPa and 630 MPa, however, the same difficulties for optical crack detection were met. Therefore, strain maps for 500 MPa were presented only, Fig. 8.

Fig. 8. Comparison of ESPI measurements performed for the stress amplitude equal to 500 MPa with the unified scale after: 100 000 cycles (a); 250 000 cycles (b); 299 207 cycles (c).

In order to check applicability of the DIC methodology, measurements were performed for the same stress amplitude as that for the ESPI used, i.e. 500 Mpa, after selected number of cycles to the specimen fracture.

Unlike the ESPI measurements, DIC technique captured a strain localisation area after just one cycle (Fig. 9a).

Fig. 9. DIC measurements performed for the stress amplitude equal to 500 MPa with unified scale after : 1 cycle (a); 100 000 cycles (b); 250 000 cycles (c); 301 251 cycles (d).

The subsequent evolution of fatigue damage to 100 000 cycles enabled to clearly indicate the area of potential crack initiation (Fig. 9b) and its development (Fig.9c-d) up to specimen fracture.The effectiveness of DIC method was further confirmed by
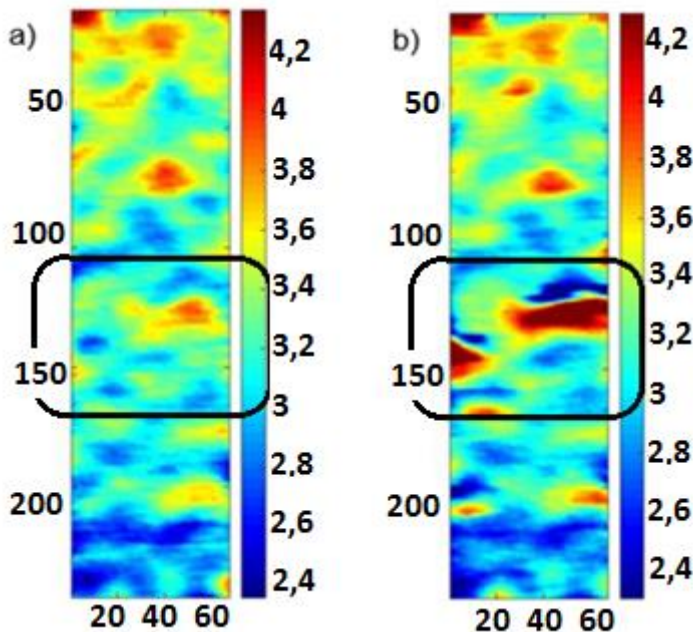
performing an additional measurements for the stress amplitude equal to 600 MPa, 630 MPa and 640 MPa. For the each measurement, the area of potential crack initiation was precisely captured after initial number of fatigue cycles and specimens fractured exactly in this specified region. It should be mentioned however, that the application of highest values of stress amplitude required to modify the scale in order to clearly present the strain distribution.

3.3. The results for the nickel super-alloy

Fatigue investigations on nickel super-alloy were also carried out under force control using the MTS-810 hydraulic testing machine. In each test the maximum cyclic stress range and stress amplitude were equal to 600 MPa and 300MPa, respectively.

The first cycle was conducted manually, and subsequently, a block of cycles under the frequency of 10 Hz was carried [19]. The process of cyclic loading was interrupted several times in order to perform displacement measurements by means of the ESPI camera. The experimental programme provided displacement measurements at the beginning of test and after 20000, 40000 and 50000 cycles. The number of cycles to failure was $N_f=54315$.

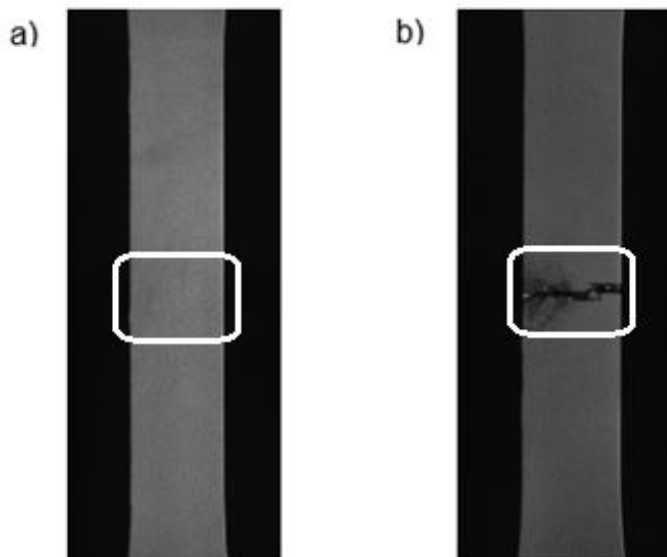**Fig. 10.** The field strain distribution along Y axis corresponding to the acting stress direction. Measurements performed: (a) in the first loading cycle; (b) after 50000 cycles. Scale is matched to the extreme strain values in the first measurement.

ESPI observations carrying out at various stages of the fatigue degradation represent a status and dynamics of the damage development. They enable a determination of
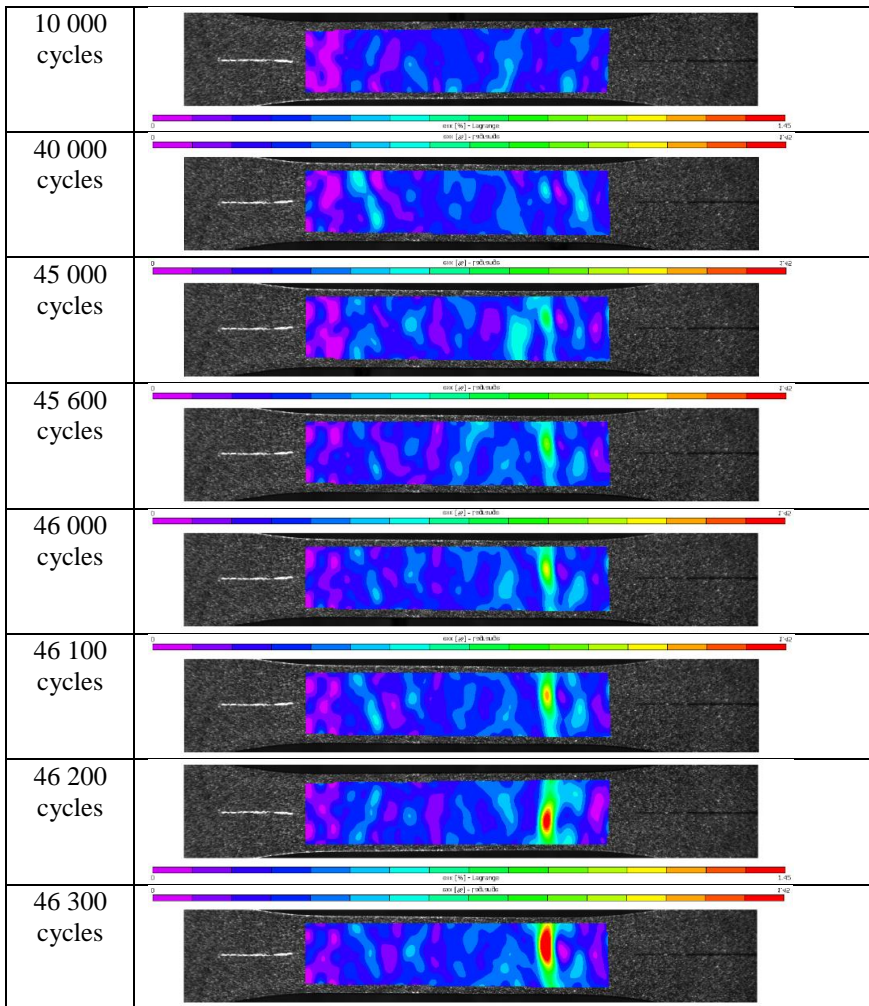
the areas of the greatest stress concentrations and reflect a local character of the fatigue damage initiation.

The field strain distributions along the vertical axis corresponding to the acting stress direction in the specimen are presented in Fig. 10. The figure shows strain distributions for different stages of the fatigue process, i.e. after: (a) first cycle; and (b) 50000 cycles. It has to be mentioned, that all these maps were obtained for the same scale in order to enable a direct comparison of the results achieved. As it is seen, the method enables identification of places where damage initiates. Figure 11 demonstrates a location of decohesion on the specimen gauge length, that well agrees with the largest displacement concentration occurring on the phase maps captured by means of the ESPI measurements.

Fig. 11. Fatigue specimen photo: (a) before fatigue test; (b) after fatigue test (N_f= 54315 cycle)

In order to find which optical technique is more suitable for damage identification for this material, similar fatigue investigations were carried out in tests supported by the DIC system. These tests were performed at stress amplitude equal to 600 MPa. The loading frequency was 20 Hz, and the image was recorded every 5 seconds, i.e. each map was recorded every 100 cycles. Figure 12 presents images from selected fatigue cycles. The specimen broke after 46 364 cycles.

10 000 cycles	
40 000 cycles	
45 000 cycles	
45 600 cycles	
46 000 cycles	
46 100 cycles	
46 200 cycles	
46 300 cycles	

Fig. 12. Images showing strain distribution maps captured by DIC

For this specimen, the first signs of localization were visible after 45 thousands loading cycles. The increase in deformation at this stage was connected with the formation of a crack in the material, which propagates until the cohesion is entirely lost. On this basis, the moment of crack formation can be estimated, although the detection threshold is lower than that in the technically comparable ESPI method obtained.

4. Conclusions

The paper presents the results of fatigue tests carried out on the P91 power engineering steel and nickel super-alloy with special emphasis on damage development

identification. Contemporary novel optical techniques were used for damage initiation detection and further crack propagation monitoring. The results of damage monitoring during fatigue tests supported by Digital Image Correlation or Electronic Speckle Pattern Interferometry proved their great suitability for effective identification of places of damage initiation.

Both optical techniques were assessed in terms of their effectiveness to fatigue damage development monitoring. It was found, that DIC enables to monitor the fatigue behaviour and accurately indicates the area of potential failure within the early stage of fatigue damage development.

Contrary to this, the application of ESPI method was not so successful. It also enabled to indicate a location of potential damage area, however, significantly later than DIC. The main limitation of ESPI technique usage results from its high sensitivity which procures many difficulties during working with the servo-controlled hydraulic testing machines. Such machines generate high frequency vibrations during experiments due to oil flow supplying the machine loading systems. The vibrations disturb significantly a work of ESPI cameras and narrows greatly its measuring capabilities.

Acknowledgements

References

[1] Ustrzycka A., Mróz Z., Kowalewski Z.L. and Kucharski S., Analysis of fatigue crack initiation in cyclic microplasticity regime, *International Journal of Fatigue*, Vol.131, pp.105342-1-15, 2020.

[2] Kopec M., Brodecki A., Kukla D. and Kowalewski Z.L., Suitability of DIC and ESPI optical methods for monitoring fatigue damage development in X10CrMoVNb9-1 power engineering steel, *Archives of Civil and Mechanical Engineering*, Vol.21, pp.167-1-13, 2021.

[3] Altenbach H., Brünig M., Kowalewski Z.L., *Plasticity, Damage and Fracture in Advanced Materials*, Springer, 2020, ISBN 978-0-030-34850-2.

[4] Andersson M., The influence of notches on fatigue of heat treated sintered steel. In: *International Powder Metallurgy Congress and Exhibition* (2013) Euro PM2013 in Gothenburg on September 17, 2013.

[5] Chu T.C., Ranson W.F., Sutton M.A., Peters W.H., Application of digital-image-correlation techniques to experimental mechanics. *Experimental Mechanics*, 25, 232–244, 1985, DOI 10.1007/BF02325092.

[6] Lord J.D., Digital image correlation (DIC). In: Eaton-Evans J., Dulie-Barton J.M., Burguete RL (eds), *Modern Stress and Strain Analysis. A State of the Art Guide to Measurement Techniques*, British Society for Strain Measurement, pp. 14–15, 2009.

[7] Forster J., Theobald A., Engel S., Pasmann R., Using optical measuring system for identification of material parameters for finite element analysis. In: *11. LS-DYNA, DYNAmore GmbH*, Ulm, pp. 1–9, 2012.

[8]   Durif E., Réthoré J., Combescure A., Fregonese M., Chaudet P., Controllingstress intensity factors during a fatigue crack propagation using digital imagecorrelation and a load shedding procedure, *Experimental Mechanics* 52, pp. 1021–1031, 2012, doi 10.1007/s11340-011-9552-6.

[9]   Han Y., Kim D.W., Kwon H.J., Application of digital image cross-correlation and smoothing function to the diagnosis of breast cancer. *J Mech Behav Biomed Mater*., 14, pp. 7–18, 2012, doi:10.1016/j.jmbbm.2012.05.007.

[10]   Hokka M., Mirow N., Nagel H., Irqsusi M., Vogt S., Kuokkala V.T., In-vivo deformation measurements of the human heart by 3D digital image correlation. *J Biomech.,* 48, pp. 2217–2220, 2015, doi:10.1016/j.jbiomech.2015.03.015.

[11]   Juszczyk M.M., Cristofolini L., Viceconti M., The human proximal femur behaves linearly elastic up to failure under physiological loading conditions. *J Biomech*., 44, pp. 2259–2266, 2011, 10.1016/j.jbiomech.2011.05.038.

[12]   Zani L., Erani P., Grassi L., Taddei F., Cristofolini L., Strain distribution in the proximal Human femur during in vitro simulated sideways fall. *J Biomech.,* 48, pp. 2130–2143, 2015, doi:10.1016/j.jbiomech.2015.02.022.

[13]   Yoon S., Jung H.-J., Knowles J.C., Lee H.-H., Digital image correlation in dental materials and related research: A review, *Dental Materials*, 37, pp. 758-771, 2021 https://doi.org/10.1016/j.dental.2021.02.024.

[14]   Berke R., Lambros J., Ultraviolet digital image correlation (UV-DIC) for high temperature applications. *The Review of Scientific Instruments*, 85, 4, 2014.

[15]   Niezrecki C., Avitabile P., Warren C., Pingle P., Helfrick M., A review of digital image correlation applied to structural dynamics, *AIP Conference Proceedings*, American Institute of Physics, 1253, pp. 219-232, 2010.

[16]   Lunt A.J.G., Korsunsky A.M., A review of micro-scale focused ion beam milling and digital image correlation analysis for residual stress evaluation and error estimation, *Surf and Coati Tech*, 283, pp. 373-388, 2015, https://doi.org/10.1016/j.surfcoat.2015.10.049.

[17]   Cunha F.G., Santos T.G., Xavier J., In Situ Monitoring of Additive Manufacturing Using Digital Image Correlation: A Review, *Materials*, 14, pp. 1511, 2021, https://doi.org/10.3390/ma14061511.

[18]   Pagliarulo V. and Ferraro P., New applications of electronic speckle pattern interferometry in novel materials and structures", *Proc. SPIE 11059, Multimodal Sensing: Technologies and Applications*, 1105910, 21 June 2019; https://doi.org/10.1117/12.2527997.

[19]   Kopec M., Grzywna P., Kukla D., Kowalewski Z., Evaluation of the fatigue damage development using ESPI method, *Inżynieria Materiałowa*, 4(212), pp.1-4, 2016.